Pergamon

Int. J. Heat Mass Transfer. Vol. 40, No. 10, pp. 2273–2281, 1997

0017-9310/97 $17.00+0.00

PII: S0017-9310(96)00315-8

Mixed convective heat and moisture transfer from a horizontal furry cylinder in a transverse wind

SRINIVAS BUDARAJU,†‡ WARREN E. STEWART†§ and WARREN P. PORTER||

† Departments of Chemical Engineering and ||Zoology, University of Wisconsin, Madison, WI 53706, U.S.A.

(*Received* 18 *July* 1995 *and in final form* 30 *August* 1996)

Abstract—Free and forced convection heat and moisture transfer are investigated for the fur layer on a model animal limb or torso in a transverse wind. The analysis includes various modes of heat transfer through dry fur: conduction through the hairs, conduction, free and forced convection in the interstitial and external air, and evaporation from the skin. The relative contributions of these mechanisms are investigated by finite-element calculations for several mammalian species. Comparisons are made with the experimental data of Gebremedhin on Holstein calves.

INTRODUCTION

Heat and mass transfer are crucial aspects of individual animal energetics, growth and reproduction potential, and survivorship. Heat and mass transfer also have important effects on animal behavior, as in foraging and predation, thus affecting animal population dynamics and community structure. Applications of heat and mass exchange consequently abound in animal husbandry, conservation biology, wildlife ecology and zoology.

In this paper, heat transfer through the fur covering of a model animal is studied, quantifying the contributions of conduction through the hairs, conduction, free and forced convection in the interstitial and external air, and evaporation from the skin. The geometry investigated is a horizontal fur-covered cylinder, representing an animal torso or limb in a transverse wind.

Free convection from a heated horizontal cylinder in a porous medium was studied by Hardee [2], Ingham and Pop [3] and Merkin [4]. Heat transfer from a porous cylinder at low Reynolds numbers was analyzed by Ramilison and Gebhart [5]. Forced or mixed convection from a horizontal cylinder embedded in an infinite porous medium was studied by several investigators [6–14] using Darcy's law. The present investigation deals with coupled mass and energy transport in the fur covering of an animal, including the anisotropy of the fibrous medium and the wind-driven convection encountered at large external Reynolds numbers.

Evaporation of water, which removes energy from the skin as latent heat, is a means of thermal regulation in animals. Vapor pressure measurements in the coats of cattle indicate that evaporative cooling occurs mainly at the skin [15]. Cena and Monteith [16] measured the diffusivity of water vapor through cured and uncured fleece from Dorset Down Sheep and through fiberglass. They found that for their thicker samples, the transport of water was assisted by capillary movement along the hairs, but the transport of energy was negligibly affected.

In a previous paper [17], we have outlined a computational scheme for predicting forced ventilation around the fur-covered cylinder shown in Fig. 1. This method assumes an anisotropic Darcy model for the fur. A measured pressure distribution for a solid cylinder is applied at the outer boundary of the fur, on the ground that the slow flow through the fur has little effect on the external flow. The permeabilities in the radial and tangential directions are approximated locally with known solutions of Stokes' equations for creeping flow through arrays of parallel cylindrical rods in equilateral triangular spacing. The local Reynolds number based on the hair diameter, $Re_h = \rho_\infty U D_h/\mu$, is less than unity throughout the fur in all the present calculations. This model of the intrafur flow is valid in the external Reynolds number range $1.5\times10^3 < Re < 1.5\times10^5$. In the following sections, we give a corresponding model for heat and moisture transport with mixed convection, and demonstrate this model with finite-element simulations for several mammalian species.

Nature designs animal fur to provide a controlling heat-transfer resistance, normally exceeding the thermal resistance of the boundary layer in the external flow. This is convenient, because the intrafur flow is laminar whereas the external flow at $Re > 1500$ is very

‡ Westvaco Research Center, Covington, VA 24426, U.S.A.

§ Author to whom correspondence should be addressed.

NOMENCLATURE

$\hat{C}_p$	heat capacity at constant pressure
D_{er}, $D_{e\theta}$	effective diffusivities in r- and θ-directions in the porous medium
D_h	hair diameter
D_{wa}	diffusivity of water vapor in air
gH	gravitational potential energy
h	heat transfer coefficient
$\boldsymbol{K}^{-1}$	flow resistance tensor
k	thermal conductivity
k_ω	mass transfer coefficient (mass basis)
L	length of furry cylinder
L_h	hair length
M	molecular weight
N	hair number density at skin
p	total pressure
$\wp$	$=p+\rho_\infty gH$, pressure function
p_v	vapor pressure of water at T_s
Q	rate of heat loss from the skin
r, θ, z	cylindrical coordinates in Fig. 1
R_f	outer radius of furry cylinder in Fig. 1
R_s	skin radius of furry cylinder in Fig. 1
Re	$=2R_f\rho_\infty U_\infty/\mu$, Reynolds number for outer flow
Re_h	$=D_h\rho_\infty U/\mu$, local Reynolds number for intrafur flow
Re_θ	$=2R_f\rho_\infty U_{\theta,\max}/\mu$, overall Reynolds number for intrafur flow
T	temperature
U	filter velocity vector in Darcy's law
$U_{\theta,\max}$	maximum value of U_θ in fur
x, y, z	rectangular coordinates in Fig. 1.

Greek symbols

ε	local porosity (fluid volume fraction) in porous medium
κ^{rr}, $\kappa^{\theta\theta}$	resistance coefficients in eqn (4)
λ	latent heat of vaporization
μ	fluid viscosity
ρ	fluid density
ψ	stream function
ω	mass fraction of water vapor.

Subscripts

a	air
f	outer boundary of the fur
h	hair
r	radial direction
s	skin surface
w	water vapor
z	z-direction
θ	θ-direction
∞	conditions far upstream of cylinder.

Superscripts

^	per unit mass
~	approximating function.

complicated, with fluctuations, vortex-shedding and turbulent regions. Here we provide a detailed treatment of the crucial intrafur region, and represent the outer region by use of measured transfer coefficients for flow across solid cylinders.

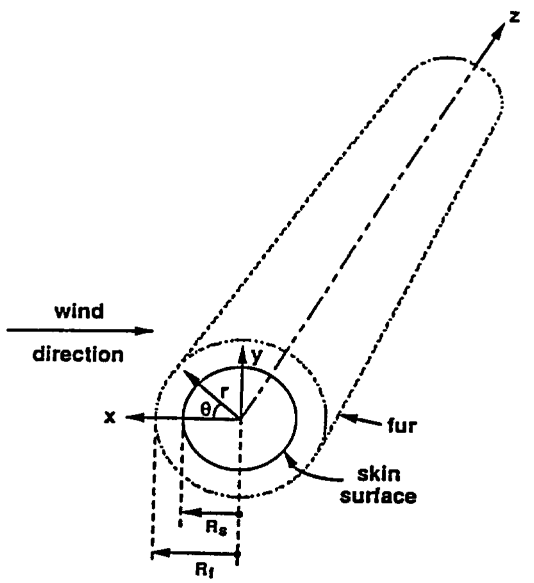

Fig. 1. Schematic view of the flow system.

SYSTEM DESCRIPTION

A fur-covered cylinder, shown in Fig. 1, is used here as a geometric model of an animal limb or torso with skin radius R_s. In the present model, the fur consists of straight, erect hairs of length L_h and diameter D_h, distributed uniformly with number density N per unit area of skin. The outer fur radius R_f is then equal to R_s+L_h. The cylinder is exposed to a transverse air stream with approach speed U_∞, ambient temperature T_∞ and water vapor mass fraction ω_∞. The skin is kept at a uniform temperature T_s. Perspiration from the skin causes cooling, and the generated water vapor is vented through the fur. We will calculate the profiles of velocity, temperature and water vapor mass fraction in the interstitial air to a pseudo-continuum approximation. We treat the physical properties of each phase as constants, except in the gravity force term ρg; this approach parallels that of Boussinesq [18].

We model the filter velocity $\boldsymbol{U}$ in the fur with Darcy's law in the form

$$[\boldsymbol{K}^{-1} \cdot \boldsymbol{U}] = (-\nabla p + \rho \boldsymbol{g})/\mu, \tag{1}$$

where $\boldsymbol{K}^{-1}$ is the flow resistance tensor, p is the local pressure, ρ is the local fluid density and $\boldsymbol{g}$ is the gravity vector. The smoothed continuity equation is approximated here as $(\nabla \cdot \boldsymbol{U}) = 0$, and solved with a stream function ψ [19], giving the expressions

$$U_\theta = \frac{\partial \psi}{\partial r}, \quad U_r = -\frac{1}{r}\frac{\partial \psi}{\partial \theta}, \tag{2, 3}$$

for the velocity components.

Taking the curl of eqn (1), with μ regarded as constant, we obtain the following differential equation for the stream function,

$$\frac{\kappa^{rr}}{r^2}\frac{\partial^2 \psi}{\partial \theta^2} + \frac{\kappa^{\theta\theta}}{r}\frac{\partial}{\partial r}\left(r\frac{\partial \psi}{\partial r}\right) + \frac{\mathrm{d}\kappa^{\theta\theta}}{\mathrm{d}r}\frac{\partial \psi}{\partial r} = \frac{g}{\mu}\left(\frac{\sin\theta}{r}\frac{\partial \rho}{\partial \theta} - \cos\theta\frac{\partial \rho}{\partial r}\right) \tag{4}$$

after use of (2, 3) and the identity curl $\nabla p \equiv 0$. The elements κ^{rr} and $\kappa^{\theta\theta}$ of the tensor $\boldsymbol{K}^{-1}$ have been tabulated as functions of local porosity by Stewart *et al.* [20]; they depend on r in the system of Fig. 1.

The local density ρ of the moist air is represented via the isobaric ideal-gas expression

$$\frac{\rho}{\rho_\infty} = \frac{MT_\infty}{M_\infty T}, \tag{5}$$

with the formula

$$\frac{1}{M} = \frac{\omega}{M_w} + \frac{1-\omega}{M_a} \tag{6}$$

for the local number-mean molecular weight M. The resulting treatment of buoyant forces is more accurate than the conventional use of a linearized equation of state.

The smoothed energy equation for the intrafur region reduces to

$$\frac{\rho_\infty \hat{C}_p}{r}\left(-\frac{\partial \psi}{\partial \theta}\frac{\partial T}{\partial r} + \frac{\partial \psi}{\partial r}\frac{\partial T}{\partial \theta}\right) = \frac{1}{r}\frac{\partial}{\partial r}\left(rk_r\frac{\partial T}{\partial r}\right) + \frac{k_\theta}{r^2}\frac{\partial^2 T}{\partial \theta^2} \tag{7}$$

in the absence of viscous dissipation. Here k_r and k_θ are effective thermal conductivities of the two-phase medium in those directions. For k_r, a volumetric average of the fluid- and solid-phase conductivities k_a and k_h suffices:

$$k_r = \varepsilon k_a + (1-\varepsilon)k_h. \tag{8}$$

The thermal conductivity k_h of hair is taken to be 0.209 W m^{-1} K^{-1} at 35°C [21]. The local fur porosity ε in eqn (8) varies with position as

$$\varepsilon = 1 - \frac{N\pi D_h^2 R_s}{4r} \tag{9}$$

for erect, cylindrical hairs of diameter D_h and number density N per unit area of skin. The results of Perrins *et al.* [22] give the tangential conductivity expression

$$\frac{k_\theta}{k_a} = 1 - \frac{2\phi_1}{\left[\phi_2 + \phi_1 - \dfrac{0.075422\phi_1^6\phi_2}{\phi_2^2 - 1.060283\phi_1^{12}} - \dfrac{0.000076\phi_1^{12}}{\phi_2}\right]} \tag{10}$$

for our system, at the local porosity ε. Here $\phi_1 = 1-\varepsilon$ and $\phi_2 = (k_a+k_h)/(k_a-k_h)$. The expression is reported to be valid for $\varepsilon > 0.3$.

The smoothed mass-fraction distribution in the fur satisfies the mass balance equation

$$\frac{1}{r}\left(-\frac{\partial \psi}{\partial \theta}\frac{\partial \omega}{\partial r} + \frac{\partial \psi}{\partial r}\frac{\partial \omega}{\partial \theta}\right) = \frac{1}{r}\frac{\partial}{\partial r}\left(rD_{er}\frac{\partial \omega}{\partial r}\right) + \frac{D_{e\theta}}{r^2}\frac{\partial^2 \omega}{\partial \theta^2}, \tag{11}$$

in which D_{er} and $D_{e\theta}$ are the effective diffusivities in the r and θ directions. The tortuosity in the radial direction is unity, hence,

$$D_{er}(r) = \varepsilon(r)D_{wa}, \tag{12}$$

in which D_{wa} is the diffusivity of water vapor in air. In the θ direction, the tortuosity is approximated as unity; refinements of this estimate were not explored, since the resulting diffusion proved to be very small.

BOUNDARY CONDITIONS

Equations (4), (7) and (11) are to be solved simultaneously using the following boundary conditions:

$$\psi|_{R_s,\theta} = 0,$$

$$\left(\mu\kappa^{\theta\theta}\frac{\partial \psi}{\partial r}\right)\bigg|_{R_f,\theta} = \left(-\frac{1}{r}\frac{\partial \wp}{\partial \theta} + (\rho_\infty - \rho)g\cos\theta\right)\bigg|_{R_f,\theta}, \tag{13, 14}$$

$$T|_{R_s,\theta} = T_s, \quad \left(-k_r\frac{\partial T}{\partial r}\right)\bigg|_{R_f,\theta} = h(T|_{R_f,\theta} - T_\infty), \tag{15, 16}$$

$$\omega|_{R_s,\theta} = \omega_s = \frac{M_w p_v}{Mp},$$

$$\left(-\rho_\infty D_{er}\frac{\partial \omega}{\partial r}\right)\bigg|_{R_f,\theta} = k_\omega(\omega|_{R_f,\theta} - \omega_\infty), \tag{17, 18}$$

$$T|_{r,\theta=0} = T|_{r,\theta=2\pi}, \quad \frac{\partial T}{\partial \theta}\bigg|_{r,\theta=0} = \frac{\partial T}{\partial \theta}\bigg|_{r,\theta=2\pi}, \tag{19, 20}$$

$$\psi|_{r,\theta=0} = \psi|_{r,\theta=2\pi}, \quad \left.\frac{\partial\psi}{\partial\theta}\right|_{r,\theta=0} = \left.\frac{\partial\psi}{\partial\theta}\right|_{r,\theta=2\pi}, \tag{21,22}$$

$$\omega|_{r,\theta=0} = \omega|_{r,\theta=2\pi}, \quad \left.\frac{\partial\omega}{\partial\theta}\right|_{r,\theta=0} = \left.\frac{\partial\omega}{\partial\theta}\right|_{r,\theta=2\pi}. \tag{23,24}$$

Equation (14) is the θ-component of eqn (1) at the outer edge of the fur. The right-hand member of eqn (14) includes the tangential buoyant force $(\rho_\infty - \rho)g\cos\theta$, and the tangential gradient of the pressure function $\wp = p + \rho_\infty gH$. The latter function is represented at R_f as $\wp_\infty + \frac{1}{2}\rho_\infty U_\infty^2 C_p(\theta)$, the expression obtained in ref. [17] from pressure measurements on a solid cylinder in transverse flow. For this use of data from a solid cylinder, we regard the fur exterior as hydraulically smooth and neglect the effect of the intrafur flow on the pressure distribution along the outer boundary. We believe that these approximations are satisfactory at external Reynolds numbers Re not greater than 1.5×10^5.

In eqn (16), h is a local or a mean heat transfer coefficient on the outer boundary, obtained by combining the free and forced convection heat transfer coefficients as suggested by Ruckenstein and Rajagopalan [23]:

$$h^3 = h_{\mathrm{forced}}^3 + h_{\mathrm{free}}^3. \tag{25}$$

Since the Prandtl and Schmidt numbers are nearly equal for mixtures of air and water vapor, the free convection can be estimated well by use of a combined Grashof number $Gr = 8R_f^3\rho_\infty|\rho_\infty - \rho_f|g/\mu^2$. Then the mean Nusselt numbers $(2hR_f/k_\omega)$ and $(2k_\omega R_f/\rho D_{\mathrm{wa}})$ can each be estimated from Fig. 13.5-1 of Bird *et al.* [19]. Similarly, mean forced convection estimates can be found from Fig. 13.3-1 of Bird *et al.* [19], while local coefficients can be obtained from Fig. 17-10 of Knudsen and Katz [24]. Then eqn (25) and its mass transport analog will give h and k_ω for mixed convection. Note that eqn (13) neglects the displacement of the streamlines by the evaporative mass flux; this is a good approximation for the problems considered here.

SOLUTION METHOD

To convert eqns (4), (7), (11) and (13)–(24) to an approximating algebraic system for digital computer solution, the following approximating expansions are used:

$$\tilde{T} = T_s + \sum_{i=2}^{NB_r}\sum_{j=1}^{NB_\theta} A_{ij}B_i(r)B_j(\theta), \tag{26}$$

$$\tilde{\psi} = \sum_{i=2}^{NB_r}\sum_{j=1}^{NB_\theta} C_{ij}B_i(r)B_j(\theta), \tag{27}$$

$$\tilde{\omega} = \omega_s + \sum_{i=2}^{NB_r}\sum_{j=1}^{NB_\theta} D_{ij}B_i(r)B_j(\theta). \tag{28}$$

Here, $B_i(r)$ and $B_j(\theta)$ are B-splines described by de Boor [25]. NB_r and NB_θ are the numbers of basis functions in the r and θ directions:

$$NB_r = L_rNCOL_r + M_r, \tag{29}$$

$$NB_\theta = L_\theta NCOL_\theta + M_\theta. \tag{30}$$

Here L_r and L_θ are the numbers of grid intervals, $NCOL_r$ and $NCOL_\theta$ are the numbers of collocation points used per interval, and M_r and M_θ are the orders of the differential equations with respect to r and θ. The total numbers of collocation grid lines then are given by

$$N_r = L_rNCOL_r, \tag{31}$$

$$N_\theta = L_\theta NCOL_\theta. \tag{32}$$

By dropping the first radial B-spline $(B_1(r))$ in eqns (26)–(28), boundary conditions (13), (15) and (17) are automatically satisfied. The approximating algebraic system then consists of $3(NB_r - 1)NB_\theta$ equations.

Equations (4), (7) and (11) were applied at $N_r \times N_\theta$ interior grid points; eqns (14), (16) and (18) at N_θ corresponding boundary points, and eqns (19)–(24) at N_r corresponding radial points. An additional six equations, needed to make the system complete, were provided by applying eqns (14), (16) and (18) at $\theta = 0$ and $\theta = 2\pi$.

The equation system presented above was solved using the breakpoints shown in Fig. 2. These breakpoints were based on the streamline pattern found for forced ventilation in Ref. [17]. Two Gaussian collocation points per interval proved adequate in both the r and θ directions, as shown in the following section.

A damped Newton method was used to solve for the unknown coefficients A_{ij}, C_{ij} and D_{ij} in eqns (26)–(28). LAPACK routines DGETRF and DGETRS [26] were used to solve the Newton iteration equations, beginning with values of zero for all the coefficients.

The heat loss from the skin is

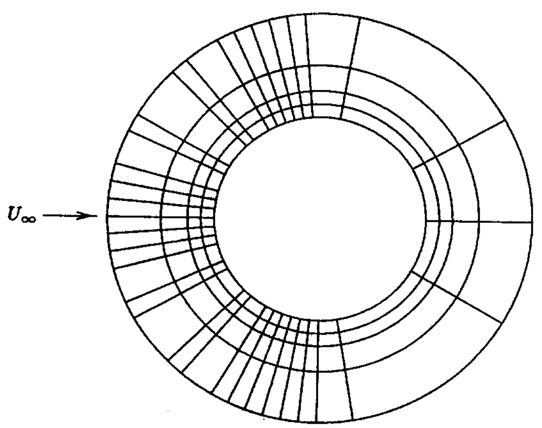

Fig. 2. Breakpoints used in the coordinates of Fig. 1.

Table 1. Characteristics of animals studied

Species	Hair diameter D_h [m]	Hair length L_h [m]	Hair density N_s [m^{-2}]	Skin radius R_s [m]
Red deer [27]	2.0×10^{-4}	4.6×10^{-2}	1.7×10^{6}	0.244
Red kangaroo [28]	1.1×10^{-4}	3.2×10^{-3}	6.2×10^{7}	0.181
Deer mouse [27]	1.0×10^{-5}	8.0×10^{-4}	1.2×10^{8}	0.030
Brushtail possum [29]	4.9×10^{-5}	1.7×10^{-2}	3.7×10^{7}	0.068
Gray squirrel [27]	8.8×10^{-5}	2.6×10^{-2}	8.0×10^{7}	0.042
Holstein calf [30]	4.6×10^{-5}	1.3×10^{-2}	5.4×10^{7}	0.216

$$Q = \int_0^{2\pi}\left(-k_r\frac{\partial T}{\partial r}\bigg|_{R_s,\theta}\right)LR_s\,\mathrm{d}\theta + \lambda\int_0^{2\pi}\left(-\rho_\infty\frac{\partial \omega}{\partial r}\bigg|_{R_s,\theta}\right)LR_s\,\mathrm{d}\theta \quad (33)$$

for a body of length L. The integrals were evaluated by Gaussian quadratures.

RESULTS AND DISCUSSION

Simulations were carried out for the mammals listed in Table 1, for a skin temperature of 310 K and an ambient temperature of 273 K. Each simulation with $NCOL_r = NCOL_\theta = 2$ took less than 3 CPU minutes on a DEC3000 workstation. Figure 3 shows computed streamlines for the red deer of Table 1 at three different wind speeds. Free convection currents can be seen clearly at low velocities, and on the rear half of the cylinder at higher velocities. Figure 4 shows calculated contours of temperature for each wind speed.

Figure 5 shows the heat loss Q as a function of wind speed U_∞ for the first five mammals of Table 1. Evaporation losses are negligible here because of the low ambient temperature (273 K). The relative contributions of conduction and forced convection within the fur depend considerably on the species and on the wind speed, but in no case is the free convection contribution important.

Table 2 demonstrates the convergence to a fine-grid limit. Here, temperature and stream function profiles are presented at four values of θ for the Holstein calf of Table 1 at wind speeds of 0.14 m s^{-1} and 4 m s^{-1} for $NCOL_r = NCOL_\theta = 1$, 2 and 3. Seven digit convergence is found at each location, verifying the sufficiency of 2×2 collocation in each element.

Table 3 shows that the use of an average heat transfer coefficient is adequate at high Reynolds numbers. Here, computations using local and average heat transfer coefficients are presented for the Holstein calf at $Re = 1.1\times10^5$. The heat loss estimates for the two cases differ by less than 4% in this example.

Computations are reported in Table 4 for several Holstein calves at a wind speed of 0.14 m s^{-1} and a relative humidity of 50% for comparison with the experimental data of Gebremedhin [1]. The fur properties of the Holstein calf (see Table 1) given by Gebremedhin *et al.* [30] were used for all the calves. The skin radii were estimated from the reported body weights assuming: (i) a body length to diameter ratio of 2.0; and (ii) a constant specific volume of 933 cm^3 kg^{-1}. The computed water loss rates correspond reasonably to measured values (see Table 4) within the typical biological variance of such experiments.

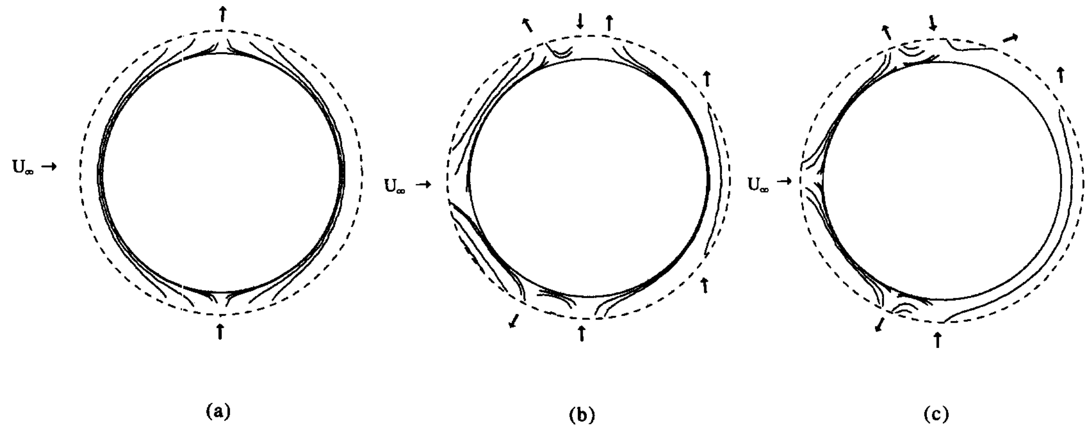

Fig. 3. Streamlines for red deer: (a) $U_\infty = 0.01$ m s^{-1}; (b) $U_\infty = 0.5$ m s^{-1}; (c) $U_\infty = 3$ m s^{-1}.

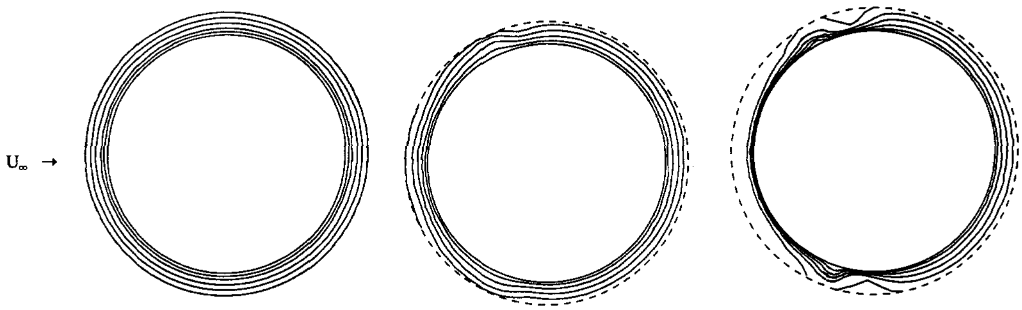

Fig. 4. Isotherms for red deer: (a) $U_\infty = 0.01$ m s^{-1}; (b) $U_\infty = 0.5$ m s^{-1}; (c) $U_\infty = 3$ m s^{-1}.

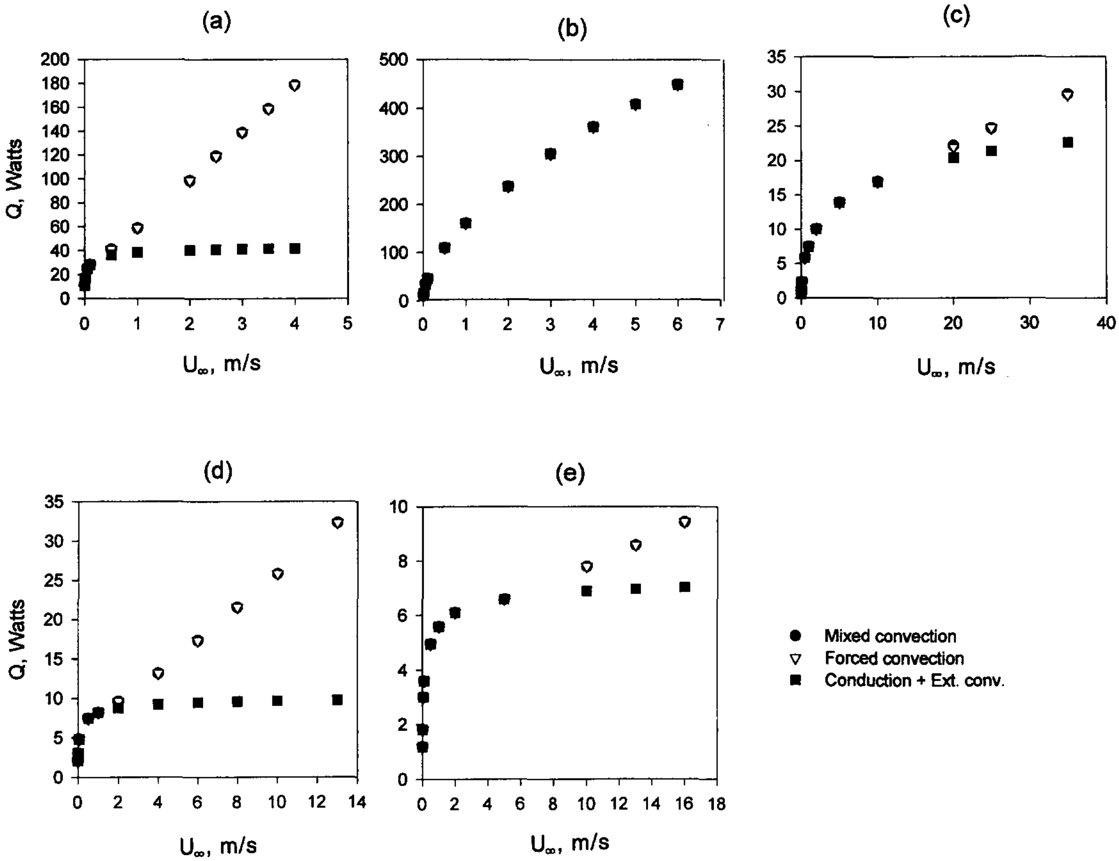

Fig. 5. Heat loss calculations for: (a) red deer; (b) red kangaroo; (c) deer mouse; (d) brushtail possum; (e) gray squirrel, with properties shown in Table 1. Body length is assumed to be four times the torso radius.

An order-of-magnitude analysis gives the conditions at which free convection is important to the fluid motion. The maximum forced-convection contribution to the filter velocity has the following magnitude, according to eqn (14) and the pressure function developed by Budaraju et al. [17]:

$$|U_{\theta,\text{forced}}| \sim \left|\frac{1}{\mu\kappa^{\theta\theta}[\varepsilon(r)]}\frac{1}{r}\frac{\partial\mathscr{P}}{\partial\theta}\right|_{R_f}$$

$$\sim \frac{1}{\mu\kappa^{\theta\theta}[\varepsilon(R_f)]R_f}\frac{\rho_\infty U_\infty^2}{2}. \quad (34)$$

The maximum free-convection contribution to the filter velocity is of the order

$$|U_{\theta,\text{free}}| \sim \frac{1}{\mu\kappa^{\theta\theta}[\varepsilon(R_f)]}|\rho_\infty - \rho|g$$

$$\sim \frac{\rho_\infty g}{\mu\kappa^{\theta\theta}[\varepsilon(R_f)]}\frac{|T_s - T_\infty|}{T_s} \quad (35)$$

for a thermally driven system, according to eqns (14), (4) and (5). Thus, the free and forced convection velocities are comparable when

Table 2. Convergence to a fine grid: calculated temperatures (K) for Holstein calf of Table 1 at $Re = 1.1 \times 10^6$

θ	$(r-R_s)/(R_r-R_s)$	$NCOL_r = NCOL_\theta = 1$	$NCOL_r = NCOL_\theta = 2$	$NCOL_r = NCOL_\theta = 3$
5°	0.2	302.1095	302.1094	302.1094
	0.4	296.2618	296.2616	296.2616
	0.6	290.4562	290.4560	290.4560
	0.8	284.6920	284.6920	284.6920
30°	0.2	302.1095	302.1094	302.1094
	0.4	296.2618	296.2616	296.2616
	0.6	290.4562	290.4560	290.4560
	0.8	284.6950	284.6920	284.6920
60°	0.2	302.1095	302.1094	302.1094
	0.4	296.2618	296.2616	296.2616
	0.6	290.4562	290.4560	290.4560
	0.8	284.6920	284.6920	284.6920
90°	0.2	302.1095	302.1094	302.1094
	0.4	296.2618	296.2616	296.2616
	0.6	290.4562	290.4560	290.4560
	0.8	284.6920	284.6920	284.6920

Table 3. Local vs mean heat transfer coefficient: calculated temperatures (K) for Holstein calf of Table 1 at $Re = 1.1 \times 10^5$

θ	$(r-R_s)/(R_f-R_s)$	Using h (local)	Using h (mean)
5°	0.2	301.9	302.1
	0.4	295.9	296.3
	0.6	289.9	290.4
	0.8	284.0	284.7
60°	0.2	302.3	302.1
	0.4	296.6	296.3
	0.6	290.9	290.4
	0.8	285.3	284.7
90°	0.2	303.0	302.1
	0.4	298.0	296.3
	0.6	293.0	290.4
	0.8	288.1	284.7
150°	0.2	301.9	302.1
	0.4	295.8	296.3
	0.6	289.8	290.4
	0.8	283.8	284.7

$$\frac{gR_f|T_s - T_\infty|}{U_\infty^2 T_s} \sim 1. \tag{36}$$

It follows that free-convection velocities in the fur are comparable with forced-convection velocities only for large mammals (body diameters > 1 m). This analysis agrees with the results presented in Figs. 3–5, and with the studies by Davis and Birkebak [31] and Fand and Phan [12].

Even when the free convection velocities are of the same order as the forced convection velocities, their effect on heat or moisture transport may not be significant. This happens at low wind velocities, where conduction through the hair fibers is more important than convection. Also, at still lower wind velocities, the diffusion flux may be larger than the convective flux for moisture transport. Conduction and convection heat losses are of the same order of magnitude when

$$Re_\theta \, Pr_r \sim 1. \tag{37}$$

Table 4. Perspiration rates of Holstein calves: comparison with the experimental data of Gebremedhin [1]

Body weight [kg]	Estimated R_s [m]	T_s [°C]	T_a [°C]	Measured rate [g h^{-1}]	Computed rate [g h^{-1}]
47.061	0.1764	37.3	29.4	221.2	202.9
47.628	0.1771	37.0	34.6	271.7	145.2
63.390	0.1948	37.3	30.6	189.0	239.6
64.864	0.1963	38.2	34.7	219.4	202.0
77.792	0.2086	38.1	30.0	193.7	294.6
78.926	0.2096	39.0	34.9	221.0	248.1
44.679	0.1734	37.6	29.5	181.2	201.6
44.906	0.1737	38.3	34.7	282.1	163.5
50.576	0.1837	37.5	30.1	101.2	214.0
51.370	0.1816	38.4	35.7	228.1	174.9
68.493	0.1999	37.9	30.1	149.7	267.4
70.308	0.2017	38.4	34.9	222.3	216.1
85.503	0.2153	38.3	30.0	201.5	317.7
87.317	0.2168	38.8	35.4	376.4	255.2
50.349	0.1804	37.7	30.1	187.5	217.2
51.143	0.1814	38.1	35.1	225.5	171.2

Here, Re_θ is the Reynolds number based on the maximum tangential velocity $U_{\theta,\max}$ [17]:

$$U_{\theta,\max} = \frac{2.83\rho_\infty U_\infty^2}{2\mu R_f \kappa^{00}(\varepsilon(R_f))}, \quad (38)$$

$$Re_\theta = \frac{2R_f\rho_\infty U_{\theta,\max}}{\mu}. \quad (39)$$

Pr_r is the radial Prandtl number given by

$$Pr_r = \frac{\hat{C}_p\mu}{k_r} \quad (40)$$

and can be several times smaller than the Prandtl number of the air. Similarly, the diffusional flux and convective mass fluxes are of the same order when

$$Re_\theta\, Sc_r \sim 1, \quad (41)$$

where Sc_r is the radial Schmidt number given by

$$Sc_r = \frac{\mu}{\rho_\infty D_{er}}. \quad (42)$$

If free convection is unimportant as determined by these criteria, eqns (4), (7) and (11) can be solved sequentially. In addition, symmetry in θ can then be exploited, thus reducing memory requirements and computation time.

Since Darcy's law (eqn (1)) is a first-order equation, its solutions exhibit slip at the boundaries. The effects of these departures from no-slip conditions are being examined by the authors.

This work is an important step toward understanding how fur coats work and how animal energy budgets are affected by fur structure and environmental factors. The results will be useful in planning the care of livestock, and in studying the survivability of wild species under various weather conditions. The principles studied here are also relevant to transport phenomena in other porous systems.

Acknowledgment—This research was supported by the National Science Foundation under Grant BSR-840523.

REFERENCES

1. Gebremedhin, K. G., Determination and modeling of heat production of calves by indirect calorimetry. Ph.D. thesis, Agricultural Engineering, University of Wisconsin, Madison, 1978.
2. Hardee, H. C., Sandia Laboratories Report, SAND 76-0075, 1976.
3. Ingham, D. B. and Pop, I., Natural convection about a heated horizontal cylinder in a porous medium. *Journal of Fluid Mechanics*, 1987, **184**, 157–181.
4. Merkin, J. H., Free convection boundary layers on axisymmetric and two-dimensional bodies of arbitrary shape in a saturated porous medium. *International Journal of Heat and Mass Transfer*, 1979, **41**, 1461–1462.
5. Ramilison, J. M. and Gebhart, B., Heat transfer from a porous cylinder immersed in a moving stream. *International Journal of Heat and Mass Transfer*, 1982, **25**, 1912–1916.
6. Huang, M., Yih, K., Chou, Y. and Chen, C., Mixed convection flow over a horizontal cylinder or sphere embedded in a saturated porous medium. *Journal of Heat Transfer*, 1986, **108**, 469–471.
7. Badr, H. and Pop, I., Combined convection from an isothermal cylinder rod buried in a porous medium. *International Journal of Heat and Mass Transfer*, 1988, **31**, 2527–2541.
8. Cheng, P., Mixed convection about a horizontal cylinder and a sphere in a fluid-saturated porous medium. *International Journal of Heat and Mass Transfer*, 1982, **25**, 1245–1246.
9. Fand, R. M., Varahasamy, M. and Greer, L. S., Empirical correlation equation for heat transfer by forced convection from cylinders embedded in porous media that account for the wall effect and dispersion. *International Journal of Heat and Mass Transfer*, 1993, **36**, 4407–4418.
10. Nasr, K., Ramadhyani, S. and Viskanta, R., An experimental investigation on forced convection heat transfer from a cylinder embedded in a packed bed. *Journal of Heat Transfer*, 1994, **116**, 73–80.
11. Hsiao, S.-W., Cheng, P. and Chen, C.-K., Non-uniform porosity and thermal dispersion effects on natural convection about a heated horizontal cylinder in an enclosed porous medium. *International Journal of Heat and Mass Transfer*, 1992, **35**, 3407–3418.
12. Fand, R. M. and Phan, R. T., Combined forced and natural convection heat transfer from a horizontal cylinder embedded in a porous medium. *International Journal of Heat and Mass Transfer*, 1987, **30**, 1351–1358.
13. Fand, R. M. and Keswani, K. K., Combined natural and forced convection heat transfer from horizontal cylinders to water. *International Journal of Heat and Mass Transfer*, 1973, **16**, 1175–1191.
14. Minkowycz, W., Cheng, P. and Chang, C., Mixed convection about a nonisothermal cylinder and a sphere in a porous medium. *Numerical Heat Transfer*, 1985, **8**, 349–359.
15. Allen, T. E., Bennett, J. W., Donegan, S. M. and Hutchinson, J. C. D., Moisture, its accumulation and site of evaporation in the coats of sweating cattle. *Journal of Agricultural Science*, 1970, **74**, 247–258.
16. Cena, K. and Montieth, J. L., Transfer processes in animal coats. III. Water vapour diffusion. *Proceedings of the Royal Society of London B*, 1975, **188**, 413–423.
17. Budaraju, S., Stewart, W. E. and Porter, W. P., Prediction of forced ventilation in animal fur from a measured pressure distribution. *Proceedings of the Royal Society of London B*, 1994, **256**, 41–46.
18. Boussinesq, J., *Theorie Analytique de la Chaleur*. Gauthier-Villars, Paris, 1903, p. 172.
19. Bird, R. B., Stewart, W. E. and Lightfoot, E. N., *Transport Phenomena*. Wiley, New York, 1960.
20. Stewart, W. E., Budaraju, S., Porter, W. P. and Jaeger, J., Prediction of forced ventilation in animal fur under ideal pressure distribution. *Functional Ecology*, 1993, **7**, 487–492.
21. Chao, B. T., *Advances in Heat Transfer*. University of Illinois Press, Urbana, 1969, p. 405.
22. Perrins, W. T., McKenzie, D. R. and McPhedran, R. C., Transport properties of regular arrays of cylinders. *Proceedings of the Royal Society of London A*, 1979, **369**, 207–225.
23. Ruckenstein, E. and Rajagopalan, R., A simple algebraic method for obtaining the heat and mass transfer coefficients under mixed convection. *Chemical Engineering Communications*, 1980, **4**, 15–29.
24. Knudsen, J. G. and Katz, D. L., *Fluid Dynamics and Heat Transfer*. McGraw-Hill, New York, 1958.
25. de Boor, C., *A Practical Guide to Splines*. Springer, New York, 1978.
26. Anderson, E., Bai, Z., Bischoff, C., Demmmel, J., Dongarra, J., Du Croz, J., Greenbaum, A., Hammarling,

S., McKenney, A., Ostrouchov, S. and Sorensen, D., *Lapack Users' Guide*, SIAM, Philadelphia, 1992.
27. Sokolov, V. E., *Mammal Skin*. University of California Press, Berkeley, 1982.
28. Dawson, J. T. and Brown, G. H., A comparison of the insulative and reflective properties of the fur of desert kangaroos. *Composite Biochemical Physiology*, 1970, **37**, 23–38.
29. Yom-Tov, Y., Green, W. O. and Coleman, J. D., Morphological trends in the common brushtail possum, *Trichosurus vulpecula*, in New Zealand. *Journal of Zoology A*, 1986, **208**, 583–593.
30. Gebremedhin, K. G., Porter, W. P. and Cramer, C. O., Quantitative analysis of the heat exchange through the fur layer of Holstein cows. *Transactions of ASAE*, 1983, **26**, 188–193.
31. Davis, Jr, L. B. and Birkebak, R. C., Convective energy transfer in fur. In *Perspectives in Biophysical Ecology*, ed. D. M. Gates and R. B. Schmerl. Springer, New York, 1975.